PLOS PATHOGENS

Comparative analysis reveals the species-specific genetic determinants of ACE2 required for SARS-CoV-2 entry

Wenlin Ren[1☝], Yunkai Zhu[2☝], Yuyan Wang[2☝], Hongyang Shi[3,4], Yin Yu[2], Gaowei Hu[2], Fei Feng[2], Xiaomin Zhao[1], Jun Lan[5], Jianping Wu[6,7], Devin J. Kenney[8], Florian Douam[8], Yimin Tong[3], Jin Zhong[3], Youhua Xie[2], Xinquan Wang[5,9], Zhenghong Yuan[2], Dongming Zhou[10], Rong Zhang[2]*, Qiang Ding[1,9]*

1 Center for Infectious Disease Research, School of Medicine, Tsinghua University, Beijing, China, 2 Key Laboratory of Medical Molecular Virology (MOE/NHC/CAMS), School of Basic Medical Sciences, Shanghai Medical College, Biosafety Level 3 Laboratory, Fudan University, Shanghai, China, 3 CAS Key Laboratory of Molecular Virology and Immunology, Institut Pasteur of Shanghai, Chinese Academy of Sciences, Shanghai, China, 4 University of Chinese Academy of Sciences, Beijing, China, 5 School of Life Sciences, Tsinghua University, Beijing, China, 6 Zhejiang Provincial Laboratory of Life Sciences and Biomedicine, Key Laboratory of Structural Biology of Zhejiang Province, School of Life Sciences, Westlake University, Hangzhou, Zhejiang, China, 7 Institute of Biology, Westlake Institute for Advanced Study, Hangzhou, Zhejiang, China, 8 Department of Microbiology, National Emerging Infectious Diseases Laboratories, Boston University School of Medicine, Boston, Massachusetts, United States of America, 9 Beijing Advanced Innovation Center for Structural Biology, Tsinghua University, Beijing China, 10 Department of Pathogen Biology, School of Basic Medical Sciences, Tianjin Medical University, Tianjin, China

☝ These authors contributed equally to this work.
* rong_zhang@fudan.edu.cn(RZ); qding@tsinghua.edu.cn(QD)

Abstract

Coronavirus interaction with its viral receptor is a primary genetic determinant of host range and tissue tropism. SARS-CoV-2 utilizes ACE2 as the receptor to enter host cell in a species-specific manner. We and others have previously shown that ACE2 orthologs from New World monkey, koala and mouse cannot interact with SARS-CoV-2 to mediate viral entry, and this defect can be restored by humanization of the restrictive residues in New World monkey ACE2. To better understand the genetic determinants behind the ability of ACE2 orthologs to support viral entry, we compared koala and mouse ACE2 sequences with that of human and identified the key residues in koala and mouse ACE2 that restrict viral receptor activity. Humanization of these critical residues rendered both koala and mouse ACE2 capable of binding the spike protein and facilitating viral entry. Our study shed more lights into the genetic determinants of ACE2 as the functional receptor of SARS-CoV-2, which facilitates our understanding of viral entry.

Author summary

SARS-CoV-2 spike protein could bind cellular receptor ACE2 for cell entry in a species-specific manner. A diverse of mammalian ACE2 proteins could be used by SARS-CoV-2 for entry, but ACE2 proteins of koala or mouse cannot bind with viral spike protein. We compared the koala or mouse ACE2 with human ACE2, and found Thr at 31 position of koala ACE2 or His at 353 position of mouse ACE2 as the restrictive residue which limits its

function as the viral receptor, respectively. Interestingly, koala or mouse ACE2 could gain the receptor function once the restrictive reside was replaced by human counterpart by genetic engineering. This study could facilitate our understanding of the genetic basis of ACE2 as the functional receptor of SARS-CoV-2, which could inform the animal model development.

Introduction

Coronaviruses, belonging to the *Orthocoronavirinae* subfamily and *Coronaviridae* family[1,2], are enveloped viruses with an approximately 30 kb, positive-sense, single-stranded RNA genome[3,4]. In the last two decades, three coronaviruses—severe acute respiratory syndrome coronavirus (SARS-CoV), Middle East respiratory syndrome coronavirus (MERS-CoV) and SARS coronavirus 2 (SARS-CoV-2)—have caused outbreaks of severe diseases in humans[5–8]. SARS-CoV-2, responsible for the ongoing COVID-19 pandemic, poses a continuing threat to global public health, especially since there are no specific and effective clinical therapeutics. To facilitate drug and vaccine development, there is an urgent need to create novel models for studying the basic biology and pathogenesis of SARS-CoV-2[9,10].

The first and essential step of virus infection is cellular receptor recognition. It has been demonstrated that the interaction of a virus with (a) species-specific receptor(s) is a primary genetic determinant of host tropism and therefore constitutes a major interspecies barrier at the level of viral entry[11–13]. SARS-CoV-2 enters host cells by binding angiotensin-converting enzyme 2 (ACE2) in a species-dependent manner[6,14,15]. Murine ACE2 does not efficiently bind the SARS-CoV-2 spike (S) protein, hindering viral entry into murine cells; consequently, human ACE2 transgenic and knock-in mice have been developed to study *in vivo* the infection and pathogenesis of SARS-CoV-2[16–19].

In exploring the host tropism of SARS-CoV-2, we and others have reported that a diverse array of ACE2 orthologs can serve as a receptor to mediate SARS-CoV-2 entry, suggesting a broad host range[20–22]. We showed that ACE2 orthologs from New World monkeys (marmoset, tufted capuchin and squirrel monkey), koalas and mouse cannot support infection with SARS-CoV-2 due to incompatibility of the S protein to the orthologs[20]. This explains, at least in part, the observation that marmosets are resistant to experimental SARS-CoV-2 infection[23]. We identified the restrictive residues at positions 41 and 42 in New World monkey ACE2 orthologs, which disrupt the formation of hydrogen bonds observed between human ACE2 and SARS-CoV-2 S protein. Replacing these two residues with the corresponding human counterparts resulted in a gain-of-function phenotype that permitted these ACE2 orthologs to act as functional SARS-CoV-2 receptors, as evidenced by binding of the viral S protein and subsequent viral entry [20]. Such findings could inform the development of marmosets as a SARS-CoV-2 infection model. Interestingly, the molecular basis for the inability of koala and mouse ACE2 to support viral entry is different from that of New World monkeys. In this study, we aimed to identify the determinants responsible for the restricted activity of koala and mouse ACE2 as a SARS-CoV-2 receptor by genetic and functional analysis. Our work could provide greater insight into the species-specific restrictions of SARS-CoV-2 cell entry.

Results

Comparative analysis identifies the potential species-specific residues in koala and mouse ACE2 that restrict SARS-CoV-2 entry

New World monkey, koala, and mouse ACE2 cannot function as a SARS-CoV-2 receptor to mediate entry, but New World monkey ACE2 humanized at residues 41 and 42 could support

viral entry[20]. To identify the genetic determinants that restrict the viral receptor activity of koala and mouse ACE2, we analyzed ACE2 orthologs (**Fig 1A**), especially the residues that interface with the SARS-CoV-2 receptor-binding domain (RBD) of the spike protein, across a diverse set of species (**Figs 1B and S1**). Based on the structure of human ACE2 complexed with the SARS-CoV-2 RBD[24–27], K31 and K353 of ACE2 are located in the contact interface with the RBD and provide a substantial amount of energy to stabilize the ACE2-spike complex [28]. Specifically, K31 and K353 form hydrogen bonds with Q493 and the carboxyl oxygen of G502 of the SARS-CoV-2 RBD, respectively. ACE2 Y83 also contributes to the interaction by forming hydrogen bonds with SARS-CoV-2 RBD N487 and Y489 as well as a π-π interaction with F486 (**Fig 1C**). However, some of these key residues differ in koala and mouse ACE2: T31 and F83 in koala, and F83 and H353 in mouse. It is conceivable that these substitutions could disrupt the interaction of these ACE2 orthologs with the viral spike and thus impair viral entry.

Humanization of restrictive residues in ACE2 orthologs rescue binding to the SARS-CoV-2 and SARS-CoV spike protein

To directly uncover the impact of these differing residues in koala and mouse ACE2 on viral entry, we introduced these residues into human ACE2, generating the following mutants: hACE2 (K31T), hACE2 (Y83F), hACE2 (K353H), hACE2 (K31T/Y83F) hACE2 (Y83F/ K353H) (**Fig 1B**). Conversely, we generated mutant koala and mouse ACE2s bearing the corresponding human residues: kACE2 (T31K), kACE2 (F83Y), kACE2 (T31K/F83Y); mACE2 (F83Y), mACE2 (H353K), mACE2 (F83Y/H353K). We then tested the ability of these mutants to bind SARS-CoV-2 S protein and mediate virus entry.

As binding of SARS-CoV-2 S protein to human ACE2 is a prerequisite for viral entry[6,14], we employed a cell-based assay using flow cytometry to assess the binding of S protein to the different ACE2 orthologs and mutants. We cloned the cDNA of our ACE2 sequences, each with a C-terminal FLAG tag, into a bicistronic lentiviral vector that expresses the fluorescent protein zsGreen1 driven by an IRES element (pLVX-IRES-zsGreen1) to monitor transduction efficiency. Next, a purified fusion protein consisting of the S1 domain of the SARS-CoV-2 S protein and an Fc domain of human IgG (S1-Fc) was incubated with A549 cells transduced with the various ACE2 lentiviruses after 48 hours transduction (**Fig 2A**). Binding of S1-Fc to ACE2 was then determined by flow cytometry as the percent of cells positive for S1-Fc among the ACE2-expressing cells (zsGreen1+ cells) (**Figs 2B and S2A and S2B**). Additionally, by immunoblotting, we confirmed that the expression of each FLAG-tagged ACE2 ortholog and variant was comparable in the transduced cells (**Fig 2C**), also with similar expression level with endogenous ACE2 in Calu-3 cells, which are permissive for SARS-CoV-2 and SARS-CoV infection (ACE2 antibody could not cross-react with koala ACE2 variants, thus only mouse ACE2 variants were used for comparison) (**S3A Fig**); Furthermore, the cell surface localization of ACE2 variants were examined by flow cytometry or confocal microscopy and our results suggest that all the ACE2 variants could localize at cell surface (**S3B–S3E Fig**). Thus, any differences in SARS-CoV-2 cell entry activity we observed were not simply due to differences in protein expression and cell surface localization.

Consistent with our previous results[20], the binding of S1-Fc to A549 cells expressing mouse or koala ACE2 was very low and comparable to levels observed in cells transduced with empty vector, whereas S1-Fc protein efficiently bound to A549 cells expressing human ACE2 (**Figs 2B and S4A**). As shown in S4A Fig, mutating human ACE2 at position 83 to the corresponding residue in mouse or koala ACE2 (Y83F) did not dramatically affect binding with SARS-CoV-2 spike (97.8% vs 98.2%) whereas substitution to the mouse residue at position 353
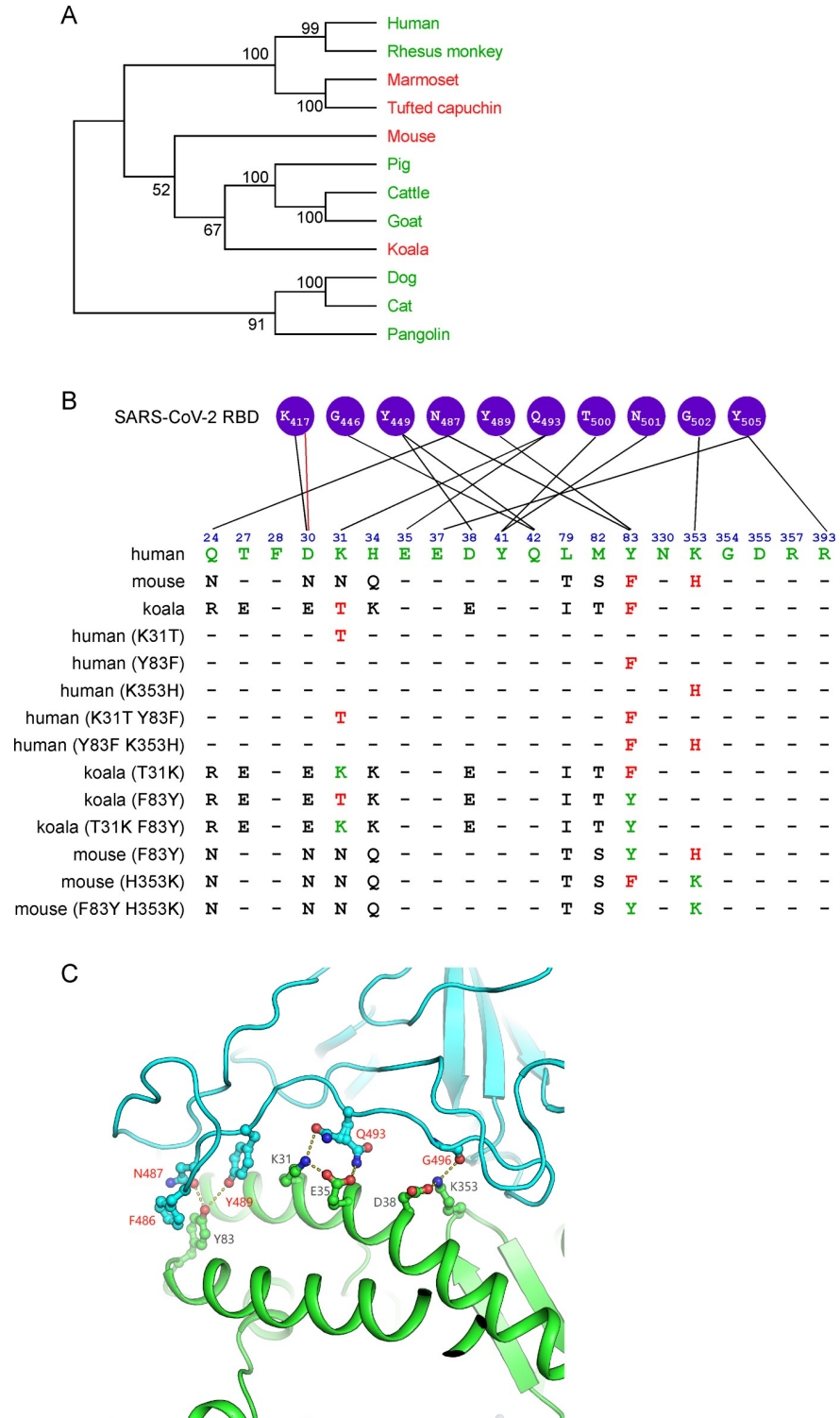
Fig 1. The potential residues in ACE2 that restrict SARS-CoV-2 entry. (A) A phylogenetic tree was constructed based on the protein sequences of ACE2 orthologs by using the Neighbor-joining method conducted in program MEGA7[40]. The percentage of replicate trees in which the associated taxa clustered together in the bootstrap test (1000 replicates) are shown next to the branches. The ACE2 sequences of these species were downloaded from NCBI, and accession numbers are shown in S1 Fig. (B) Alignment of the residues of human, koala and mouse ACE2 at the interface of ACE2 with the SARS-CoV-2 spike protein (first three rows). The restrictive residues of koala or mouse ACE2 are highlighted in red. The favorable residues of human ACE2 are highlighted in green. A series of mutant

ACE2 orthologs bearing restrictive or favorable residues were constructed in this study (remaining rows). (C) Cartoon of the binding interface between human ACE2 and the SARS-CoV-2 receptor-binding domain (RBD) (PDB code: 6M0J). ACE2 and the SARS-CoV-2 RBD colored in green and cyan, respectively. Key residues (K31, Y83, and K353) discussed in this study and their interacting residues are shown as ball-and-stick representations.

(K353H) decreased binding (74.1% vs 97.8%). Of note, the human-to-mouse hACE2 Y83F/ K353H double mutant significantly decreased binding (49.3% vs 97.8%). The human-to-koala single hACE2 K31T mutant had dramatically impaired binding (51.8% vs 97.8%) that was further reduced with mutation of residue 353 (K31T/K353H; 27.6% vs 97.8%), indicating that K31 is critical for the ACE2-spike interaction.

To gain further insights into the genetic determinants of ACE2 as the SARS-CoV-2 receptor, we examined the binding of our humanized mouse or koala ACE2 mutants with the S1-Fc protein (**Fig 2A**). The humanized mouse or koala ACE2 mutated at residue 83 (mACE2 F83Y, kACE2 F83Y) did not show increased binding efficiencies compared to wild-type mouse or koala ACE2 (1.3% vs 0.8%; 1.8% vs 1.2%, respectively) (**Fig 2B,** left panel; **S2A Fig**). However, the other singly humanized mutants (mACE2 H353K and kACE2 T31K) exhibited significantly improved binding with SARS-CoV-2 S1 protein (50.3% and 73.8%, respectively). Notably, the doubly humanized mouse (mACE2 F83Y/H353K) and koala (kACE2 T31K/F83Y) mutants demonstrated even greater binding efficiencies (83.9% and 92.1%). Together, these results indicate that although the F83Y mutation by itself had minimal effect on the binding of mouse or koala ACE2 to SARS-CoV-2 S1 protein, combining this mutation with H353K or T31K, respectively, had a synergistic effect, greatly enhancing interaction with the viral S1 to levels approaching that of human ACE2. Thus, we identified residue 353 in mouse ACE2 and residue 31 in koala ACE2 as the genetic basis for the species-specific restriction of these two orthologs in binding the SARS-CoV-2 S1.

To determine whether these observations were specific to the SARS-CoV-2 S1 protein, we also assessed the abilities of these mutants to bind the SARS-CoV S1 protein. In contrast to SARS-CoV-2 spike, mouse ACE2 could bind SARS-CoV spike (40.4% vs 0.8%) (**Fig 2B,** right panel; **S2B Fig**). Single or double mutations (F83Y, H353K or F83Y/H353K) in mouse ACE2 further increased binding efficiency (63.7%, 83.1% or 81.8%, respectively), at times even exceeding that of human ACE2 (64.0%) (**Fig 2B,** right panel). This is in line with previous reports that humanizing four residues in rat ACE2 (82–84 and 353) converted this ortholog to an efficient SARS-CoV receptor [29,30]. Intriguingly, unlike the SARS-CoV-2 spike, WT or humanized koala ACE2 displayed negligible binding to the SARS-CoV S1 (**Fig 2B,** right panel). This phenomenon was also observed using full-length spike proteins of SARS-CoV-2 and SARS-CoV (**S4B Fig**), which could exclude the S1 protein specific artifacts. To further understand the differences of SARS-CoV-2 and SARS-CoV spike protein binding with humanized koala ACE2, we analyzed the complex structures of SARS-CoV or SARS-CoV-2 RBDs with human ACE2[24,31]. The overall structure of the complex between SARS-CoV RBD and ACE2 is very similar to that between SARS-CoV-2 RBD and ACE2, with an r.m.s.d. of about 0.46 Å when they were superimposed. However, the local interactions near K31 of ACE2 is different (**Fig 2D**). K31 of ACE2 forms hydrogen bonds with E484 and Q493 from SARS-CoV2 RBD. These interactions are not conserved between SARS-CoV RBD and ACE2, as the corresponding residues P470 and N479 on SARS-CoV RBD cannot form hydrogen bond with K31 of ACE2 or is further away from K31, respectively (**Fig 2D**). The local structural difference thus provides the molecular determinant of the binding of T31K mutant of koala ACE2 to SARS-CoV-2 RBD but not SARS-CoV RBD. These observations imply that although SARS-CoV and SARS-CoV-2 both share ACE2 as the cellular receptor for entry, there are functionally important differences in receptor interaction and recognition.
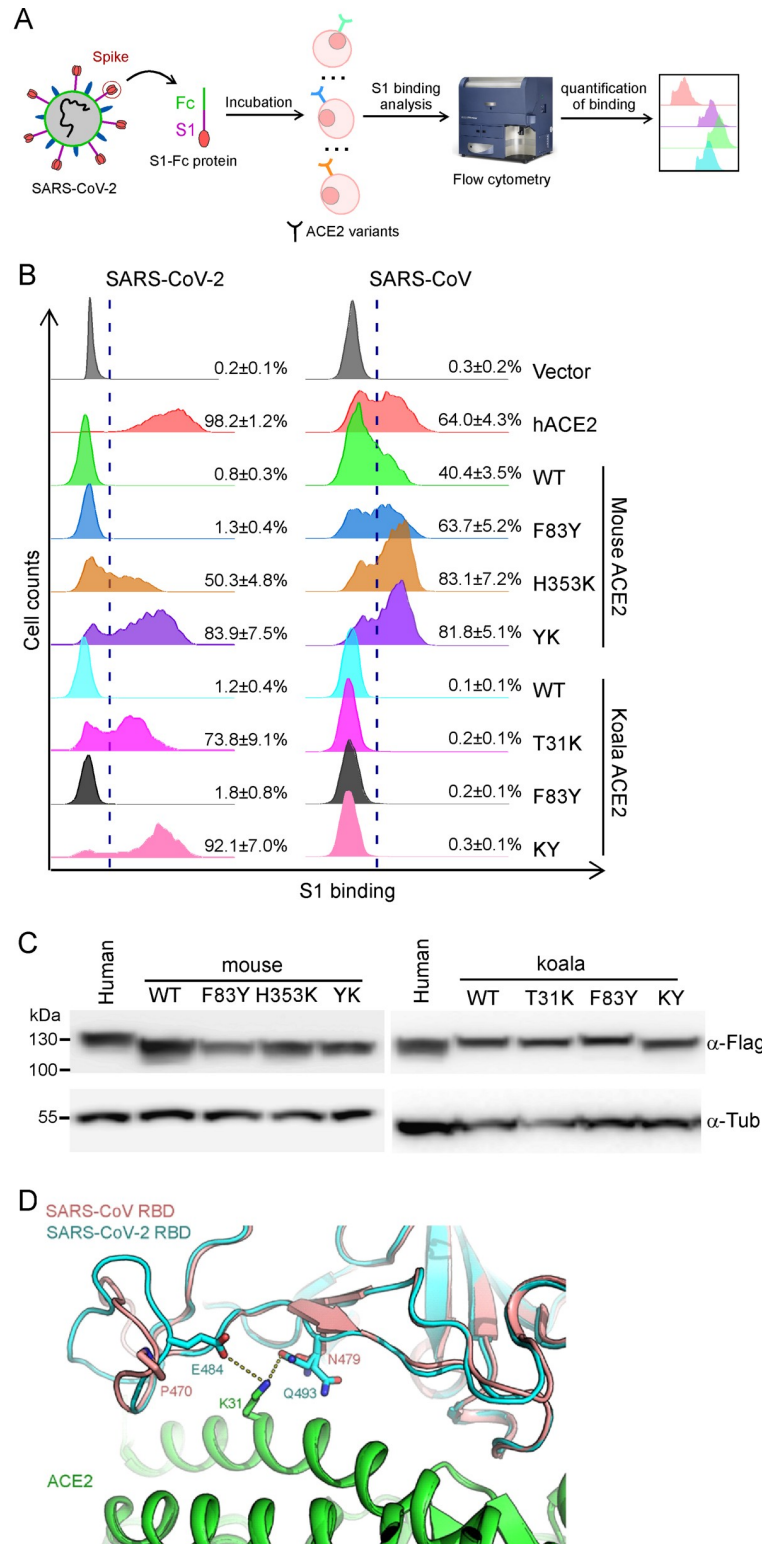
Fig 2. ACE2 mutants bind viral spike protein. (A-B) A549 cells were transduced with ACE2 orthologs or their mutants as indicated, incubated with the recombinant S1 domain of the SARS-CoV-2 or SARS-CoV spike protein C-terminally fused with Fc, and then stained with goat anti-human IgG (H + L) conjugated to Alexa Fluor 647 for flow cytometry analysis. Values are expressed as the percent of cells positive for S1-Fc among the ACE2-expressing cells

(zsGreen1+ cells) and shown as the means ± SD from 3 biological replicates. This experiments were independently performed three times with similar results. (C) Representative immunoblots A549 cells transduced with lentiviruses expressing FLAG-tagged ACE2 orthologs and humanized mutants were subjected to immunoblotting. Tubulin served as the loading control. This experiments were independently performed twice with similar results. (D) The structure of SARS-CoV RBD/ACE2 complex[31] (PDB: 2AJF) and SARS-CoV-2 RBD/ACE2[24] (PDB: 6M0J) were selected for comparison. SARS-CoV RBD, SARS-CoV-2 RBD and ACE2 are colored salmon, cyan and green, respectively. K31 of ACE2 and its adjacent residues on SARS-CoV RBD or SARS-CoV2 RBD are shown as sticks.

Genetic modification of koala and mouse ACE2 renders cells susceptible to SARS-CoV-2 pseudovirus

Next, we sought to test whether ectopic expression of our ACE2 variants were functional and could promote entry of MLV retroviral particles (Fluc as the reporter) pseudotyped with the SARS-CoV-2 spike protein into A549 cells. For comparison, we also included VSV-G and SARS-CoV spike pseudotyped virons. A549 cells expressing the ACE2 variants were inoculated with the different pseudoparticles. At 48h after inoculation, the cells were lysed and the luciferase activity assayed to determine pseudovirus entry. As expected, VSVGpp readily infected all cells with similar efficiencies independent of which ACE2 ortholog or variant was expressed (Fig 3, dark gray columns). Compared to vector-transduced A549 cells, expression of human ACE2, but not mouse or koala, enhanced the entry of SARS-CoV-2 pseudoparticles (Fig 3A and 3B, black columns). These data were in line with the binding efficiencies of these ACE2 proteins we observed with the SARS-CoV-2 spike (Fig 2B). Neither the mouse nor the koala F83Y ACE2 variant significantly increased viral entry compared to the WT ortholog; in contrast, mACE2 H353K and kACE2 T31K each significantly enhanced viral entry, and the increased entry was maintained in the doubly humanized mutants (Fig 3A and 3B).

As shown above (Fig 2B), SARS-CoV spike could bind mouse, but not koala, ACE2, and humanization of koala ACE2 at position 31 and/or 83 did not enhance binding with the SARS-CoV spike, unlike SARS-CoV-2. To further validate this observation, we tested the capabilities of ACE2 orthologs and their humanized versions to mediate SARS-CoV pseudoparticle entry. Consistent with the spike binding data, mouse ACE2 and its humanized mutants could mediate SARS-CoV pseudoparticle entry; however, the koala ACE2 mediated SARS-CoV entry with very low efficiency that was not enhanced with the T31K and/or F83Y variants (Fig 3C, light gray bars).

Collectively, the function of our ACE2 orthologs and their humanized mutants to mediate SARS-CoV-2 or SARS-CoV pseudoparticle entry corresponded with their ability to bind the respective viral spike proteins. Humanization of mouse or koala ACE2 by alteration of one or two amino acids resulted in the ability to mediate SARS-CoV-2 entry. Interestingly, humanized mouse, but not koala, ACE2 could bind the SARS-CoV and SARS-CoV-2 spike proteins and mediate entry of pseudotyped particles for each. In contrast, humanization of koala ACE2 could bind only the SARS-CoV-2 spike protein and mediate entry of only particles pseudotyped with this protein. These observations highlight the different mechanisms used by SARS-CoV and SARS-CoV-2 for entry via ACE2.

Humanization of restrictive residues in koala and mouse ACE2 orthologs renders cells susceptible to authentic SARS-CoV-2 infection

To directly test the ability of ACE2 orthologs to mediate SARS-CoV-2 entry during viral infection, we performed a genetic complementation experiment in A549 cells that lack endogenous ACE2 expression and are not susceptible to SARS-CoV-2 infection[32].

A549 cells ectopically expressing our individual ACE2 orthologs or mutants were infected with SARS-CoV-2 (MOI = 1). At 48 h post-infection, the complemented A549 cells were fixed
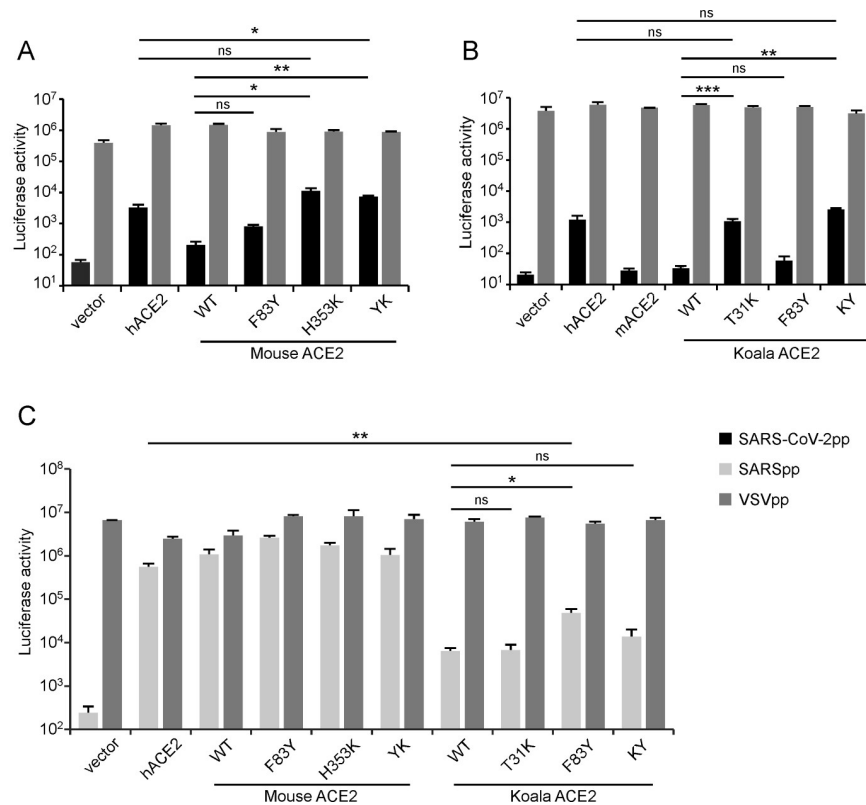
Fig 3. Ability of ACE2 orthologs and their humanized mutants to mediate entry of SARS-CoV-2 and SARS-CoV pseudoparticles. A549 cells transduced with mouse ACE2, koala ACE2 or their humanized mutants were infected with SARS-CoV-2 (A-B) or SARS-CoV (C) pseudoparticles. Two days after infection, cells were lysed and luciferase activity determined. VSV pseudoparticles were used as the control. All infections were performed in triplicate, and the data are representative of two independent experiments (mean ± standard deviation). ns, no significance; *, P < 0.05, **, P < 0.01, ***, P < 0.001. Significance assessed by one-way ANOVA.

and underwent immunofluorescent staining for intracellular viral nucleocapsid protein, an indicator of virus replication, and the cell culture medium was collected to quantify the infectious progeny virus production by titration assay (**Fig 4A**). As expected, A549 cells expressing mouse or koala ACE2 were not susceptible to SARS-CoV-2 infection while those expressing human ACE2 were susceptible (**Fig 4B**). Consistent with the data from our binding and SARS-CoV-2 pseudoparticle experiments, A549 cells expressing humanized koala (T31K) or mouse (H353K) ACE2 were readily susceptible to SARS-CoV-2 infection; as expected, the F83Y mutation in koala (T31K) or mouse (H353K) ACE2 further enhanced infection efficiency. However, the F83Y single mutation in mouse or koala ACE2 had limited function (**Fig 4B and 4C**). No or limited infectious virus can be detected from mouse ACE2, koala ACE2 and koala ACE2 F83Y transduced A549 cells (Limit of detection (LOD) = 100 FFU/ml), about 3.8×10^3 FFU/ml virus can be produced by A549 cells transduced with mouse ACE2 F83Y; 1×10^4–1×10^5 FFU/ml infectious virus were detected in A549 cells transduced with koala ACE2 T31K, koala ACE2 KY, mouse ACE2 H353K and mouse ACE2 YK variants (**Fig 4D**), which was in line with N staining results in A549 cells transduced with ACE2 variants (**Fig 4B and 4C**). Collectively, our results demonstrate that mouse and koala ACE2 with genetic humanization in the identified restrictive residues confer susceptibility to authentic SARS-CoV-2 infection.
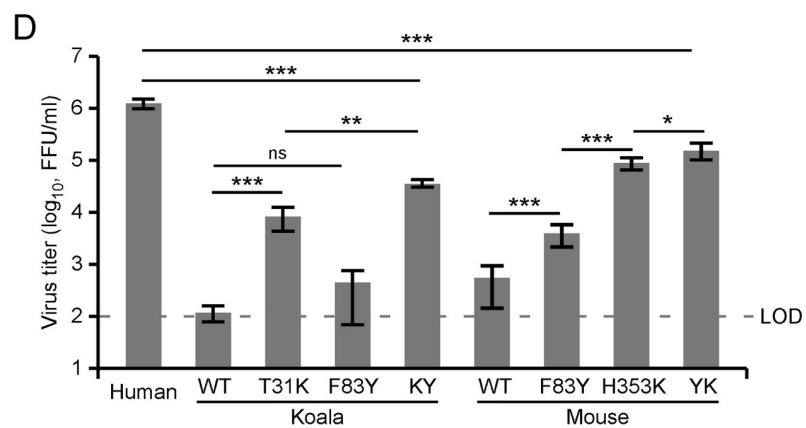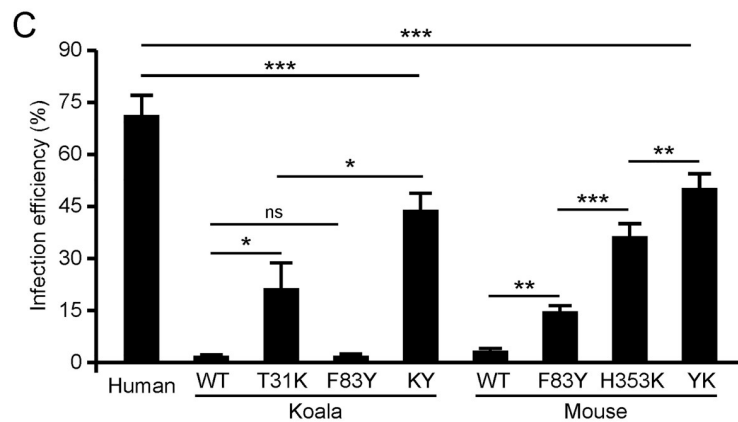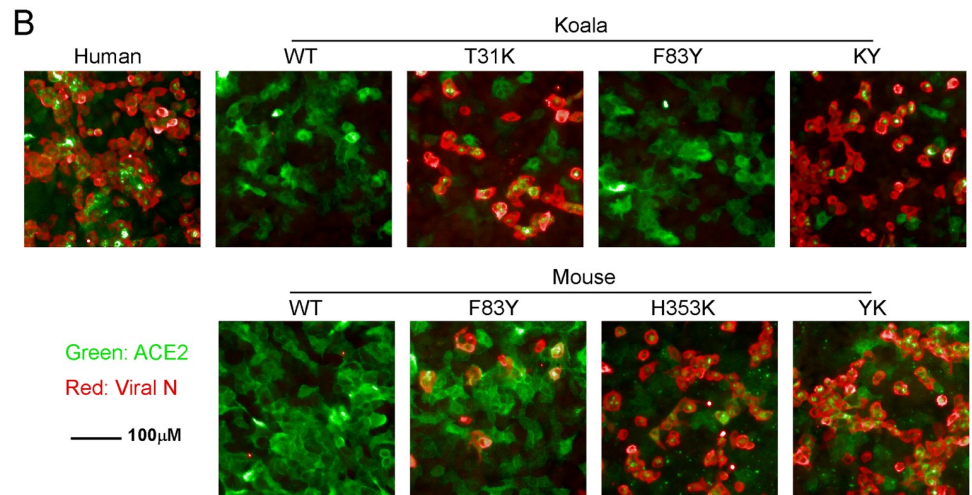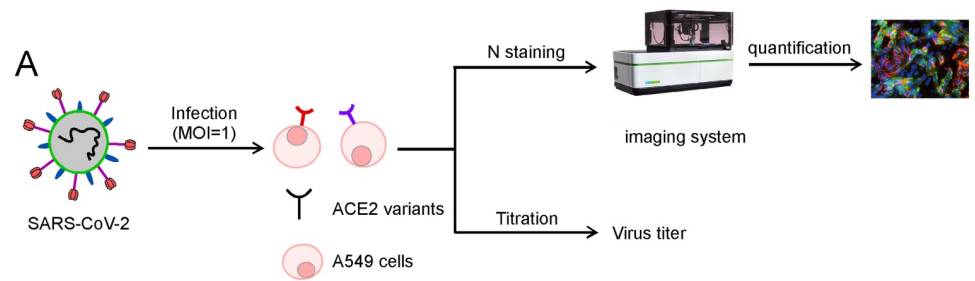
Fig 4. The capability of ACE2 mutants to facilitate viral entry *in vitro*. (A-B) A549 cells transduced with lentiviruses expressing ACE2 orthologs or humanized mutants were infected with SARS-CoV-2 virus (MOI = 1). Expression of the viral nucleocapsid protein was visualized by immunofluorescence microscopy. Viral nucleocapsid (N) (red), and ACE2 (green) are shown. (C) The infection was quantified by a high-content imaging system. (D) The cell culture medium was collected and then virus titer was determined by focus-forming assay. The graph shows the mean and SD (mean ± standard deviation) from two independent experiments performed in triplicate. ns, no significance; *, $P < 0.05$, **, $P < 0.01$, ***, $P < 0.001$. Significance assessed by one-way ANOVA.

Humanized mouse ACE2 could function as SARS-CoV-2 receptor *in vivo*

The activity of humanized mouse ACE (F83Y H353K, YK) was further evaluated *in vivo* using the adenovirus-transduced mouse model. The mice were transduced intranasally with replication-defective adenovirus encoding a functional human ACE2, which sensitized them to productive SARS-CoV-2 infection and pneumonia[33,34]. To do this, BALB/c mice were first transduced intranasally with recombinant adenovirus expressing the C-terminally FLAG-tagged human ACE2, mouse ACE2, or humanized mouse ACE2 (YK) followed by infection intranasally with SARS-CoV-2. The mice were sacrificed and lung tissues were collected for histopathological examination, viral antigen detection, and viral load titration by focus-forming assay (**Fig 5A**). In general, as compared to the mice transduced with mouse ACE2 or empty vector, we detected mononuclear cell infiltrate and protein-rich fluid exudate in lung tissue sections from mice transduced with hACE2 or mACE2 YK (**Fig 5B**). To examine the exogenous ACE2 expression delivered by adenovirus and viral antigen spread in the lungs, we performed immunochemical staining with FLAG antibody or viral N antibody. ACE2 variants were clearly detected in lung tissues collected from mice transduced with mACE2, hACE2, or mACE2 YK, whereas viral N antigen could only be detected in those of mice transduced with hACE2 and mACE2 YK (**Fig 5C**). Notably, high level of SARS-CoV-2 infectious virus was detected in lung tissue homogenates that were transduced with hACE2 or mACE2 YK (about 1×10^5 FFU/lung tissue per gram), whereas virtually none or minimal was detected in that of mice transduced with mACE2 or vector (**Fig 5D**). Taken together, our results demonstrate that humanization of mouse ACE2 by replacing the restrictive residues with human counterparts could render its viral receptor activity both *in vitro* and *in vivo*.

Discussion

The host range of coronavirus is primarily determined by its interaction with cellular receptors[3,11,12,35,36]. SARS-CoV-2 utilizes ACE2 as the receptor to enter host cells, and it has been shown that a wide range of ACE2 orthologs from mammals can bind viral spike protein to facilitate entry[20–22,37]. However, New World monkey, koala, and mouse ACE2 exhibit limited support for SARS-CoV-2 entry[20], and the underlying molecular mechanisms governing such restrictions are poorly understood. In this study, we conducted a systematic analysis of the genetic determinants of ACE2 that restrict the usage of koala and mouse ACE2 by SARS-CoV-2 for entry. We found that the genetic determinants responsible for the inability of koala and mouse ACE2 to support SARS-CoV-2 entry differ from those of New World monkeys (residues 41 and 42)[20]. Our analysis identified the restrictive residues of koala and mouse ACE2 in positions 31 and 353, respectively. Of note, humanization of koala or mouse ACE2 at either of these residues allowed these orthologs to bind viral spike proteins and mediate viral entry. Similarly, our previous study found that humanization of ACE2 from New World monkeys at positions 41 and 42 also resulted in gain-of-function phenotype[20]. Thus, together, our studies establish positions 31 (Lys), 41/42 (Tyr/Gln) and 353 (Lys) as genetic determinants regulating the usage of ACE2 as a receptor for SARS-CoV-2 infection (**Fig 6**). These data suggest that non-susceptible species have evolved species-specific mechanisms to
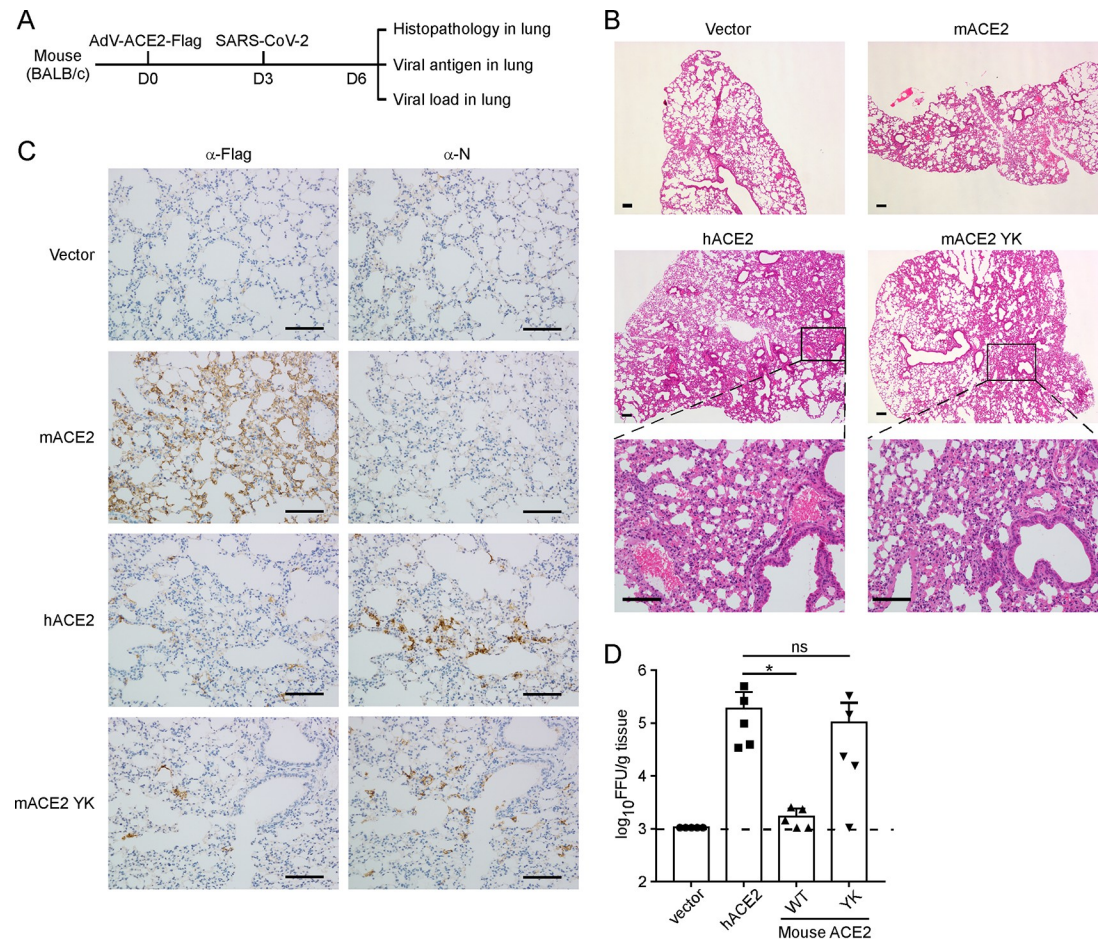
Fig 5. The humanized mouse ACE2 mediate viral entry in vivo. (A) Schematic representation of the experiment timeline; (B-D) The wild-type mice were transduced by recombinant adenovirus expressing ACE2 variants for 3 days, followed by SARS-CoV-2 challenge. Mice were sacrificed at day 3 post infection (n = 5 mice per group) and lung tissues were collected for H&E staining (B), immunostaining (C), and viral load titration (D). The ACE2 and viral N antigen expression were detected with anti-FLAG and anti-N serum, respectively. Representative images are shown from n = 5 mice. Scale bar, 100μm (B and C). Viral load was determined by focus-forming assay. ns, no significance; *, P < 0.05. Significance assessed by one-way ANOVA (D).

restrict viral entry, and it is important to understand such mechanisms to develop novel animal models for SARS-CoV-2 research.

ACE2 is a major host factor determining the host range and tissue tropism of SARS-CoV-2 infection[13,14,20,26]. Our comparative analysis of the sequences and viral receptor activities of susceptible (human) or non-susceptible (koala and mouse) ACE2 orthologs sheds more light on understanding how ACE2 mediates SARS-CoV-2 entry and defines the species-specific genetic determinants of ACE2 governing viral receptor activity. Interestingly, we also compared the susceptibility of these orthologs and their humanized mutants to SARS-CoV. We found that mouse ACE2 bound SARS-CoV spike and mediated SARS-CoV pseudovirus entry, albeit with lower efficiency than human ACE2 (**Figs 2B and 3C**), but it did not bind SARS-CoV-2 spike (**Figs 2B and 3A**). Notably, koala ACE2 could not bind SARS-CoV or SARS-CoV-2 spike. Humanizing koala ACE2 rendered the protein only able to support SARS-CoV-2, but not SARS-CoV, entry as evidenced by our cell-based binding and pseudo-viron entry experiments. These findings highlight the molecular roles of different residues of ACE2 in binding of SARS-CoV and SARS-CoV-2.
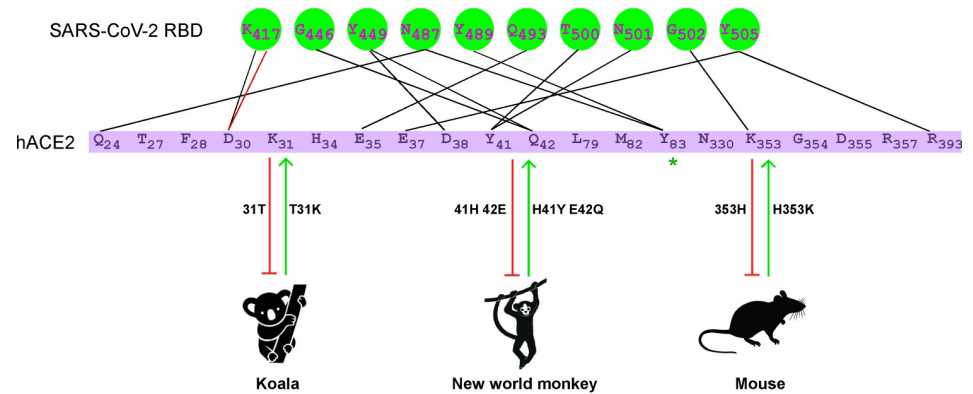
Fig 6. The genetic determinants of ACE2 required for SARS-CoV-2 entry. Mouse, koala, and New World monkey ACE2 cannot serve as functional receptors to support SARS-CoV-2 entry, as determined by different genetic restrictions. Position 31 in koala ACE2 is Thr whereas that in human is Lys. Substitution of Thr with Lys in koala ACE2 allowed for binding to the SARS-CoV-2 spike and viral entry. Different from koala ACE2, the genetic restriction of mouse ACE2 His353. Lys353 in human ACE2 can hydrogen bond with Gly502 of the SARS-CoV-2 spike protein, stabilizing the ACE2-spike complex. The presence of His at this position in mouse ACE2 disrupts this interaction. However, humanization of mouse ACE2 at position 353 renders the protein supportive of SARS-CoV-2 entry. The genetic determinants of New World monkey ACE2 were localized at positons 41 and 42 as we previously reported[20]. Thus, three genetic determinants of the ability of ACE2 to serve as the SARS-CoV-2 receptor were identified by comparative analysis of ACE2 orthologs, and the receptor activities of normally non-susceptible ACE2 orthologs could be rescued by genetic modification.

It has been well established that mice are not readily infected by SARS-CoV-2 because mouse ACE2 does not bind with SARS-CoV-2 RBD domain to mediate viral entry[6,20]. It has been reported that adaptation of SARS-CoV-2 in the mouse was dependent on a critical amino acid change, Asn501 to Tyr (N501Y), within the receptor-binding domain of the viral spike protein could render the adapted virus the capability to utilize mouse ACE2 as the receptor[38]. Recently, the mink adapted virus were also found and the adapted mutations were identified in the RBD domain; in addition the mink adapted virus could still infect human[39]. Based on this, it is conceivable that SARS-CoV-2 genome is fast-evolving and it can overcome the genetic barrier to extend its host range. As our previous and current study have been demonstrated that New world monkey[20], koala or mouse ACE2 has a low genetic barrier to restrict virus entry, and it is possible that the adapted virus in these related species could emerge in the future, which could potentially escape the vaccines and neutralizing antibodies.

Altogether, our study sheds more light on the species-specificity of interactions between SARS-CoV-2 and its cellular receptor ACE2 and uncovers evidence for a molecular arms race between SARS-CoV-2 and animal species. Here we identified the genetic basis defining the host range of SARS-CoV-2, which could potentially inform the development of novel animal models for SARS-CoV-2 research.

Materials and methods

Ethics statement

This animal experiment protocol (SARS-CoV-2 infection of adenovirus transduced mice) has been approved by the Animal Ethics Committee of School of Basic Medical Sciences at Fudan University.

Cell culture and SARS-CoV-2 virus

HEK293T (American Tissue Culture Collection, ATCC, Manassas, VA, CRL-3216), Vero E6 (Cell Bank of the Chinese Academy of Sciences, Shanghai, China) and A549 (ATCC) cells

were maintained in Dulbecco's modified Eagle medium (DMEM) (Gibco, NY, USA) supplemented with 10% (vol/vol) fetal bovine serum (FBS), 10mM HEPES, 1mM sodium pyruvate, 1×non-essential amino acids, and 50 IU/ml penicillin/streptomycin in a humidified 5% (vol/vol) CO_2 incubator at 37˚C. Cells were tested routinely and found to be free of mycoplasma contamination. The SARS-CoV-2 strain nCoV-SH01 (GenBank accession no. MT121215) was isolated from a COVID-19 patient and propagated in Vero E6 cells for use. All experiments involving virus infections were performed in the biosafety level 3 facility of Fudan University following all regulations.

Plasmids

The cDNAs encoding the ACE2 orthologs were synthesized by GenScript and cloned into the pLVX-IRES-zsGreen1 vector (Catalog No. 632187, Clontech Laboratories, Inc) with a C-terminal FLAG tag. ACE2 mutants were generated by Quikchange (Stratagene) site-directed mutagenesis. All constructs were verified by Sanger sequencing.

Lentivirus production

Vesicular stomatitis virus G protein (VSV-G) pseudotyped lentiviruses expressing ACE2 orthologs tagged with FLAG at the C-terminus were produced by transient co-transfection of the third-generation packaging plasmids pMD2.G (Addgene #12259) and psPAX2 (Addgene #12260) and the transfer vector with VigoFect DNA transfection reagent (Vigorous) into HEK293T cells. The medium was changed 12 h post transfection. Supernatants were collected at 24 and 48h after transfection, pooled, passed through a 0.45-μm filter, and frozen at -80˚C.

Western blotting

Sodium dodecyl sulfate-polyacrylamide gel electrophoresis (SDS-PAGE) immunoblotting was performed as follows: After trypsinization and cell pelleting at $2,000 \times g$ for 10 min, whole-cell lysates were harvested in RIPA lysis buffer (50 mM Tris-HCl [pH 8.0], 150mM NaCl, 1% NP-40, 0.5% sodium deoxycholate, and 0.1% SDS) supplemented with protease inhibitor cocktail (Sigma). Lysates were electrophoresed in 12% polyacrylamide gels and transferred onto nitrocellulose membrane. The blots were blocked at room temperature for 0.5 h using 5% nonfat milk in 1× phosphate-buffered saline (PBS) containing 0.1% (v/v) Tween 20. The blots were exposed to primary antibodies anti-β-Tubulin (CW0098, CWBIO), anti-FLAG (F1804, Sigma) or anti-ACE2 (Sino Biological Inc. China, Cat: 10108-T24) in 5% nonfat milk in 1× PBS containing 0.1% Tween 20 for 2 h. The blots were then washed in 1× PBS containing 0.1% Tween 20. After 1h exposure to HRP-conjugated secondary antibodies, subsequent washes were performed and membranes were visualized using the Luminescent image analyzer (GE).

Surface ACE2 binding with S1-Fc assay

A549 cells were transduced with lentiviruses expressing the ACE2 of different species for 48 h. The cells were collected with TrypLE (Thermo #12605010) and washed twice with cold PBS. Live cells were incubated with the recombinant proteins, the S1 domain of the SARS-CoV-2 spike C-terminally fused with Fc (Sino Biological #40591-V02H, 1μg/ml) or S1 domain of the SARS-CoV-2 spike C-terminally fused with mFc (Sino Biological #40150-V05H1, 1μg/ml), at 4˚C for 30 min. After washing, cells were stained with goat anti-human IgG (H + L) conjugated with Alexa Fluor 647 (Thermo #A21445, 2 μg/ml) or goat anti-mouse IgG (H + L) conjugated with Alexa Fluor 568 (Thermo #A11004, 2 μg/ml) for 30 min at 4˚C. Cells were then washed twice and subjected to flow cytometry analysis (Thermo, Attune NxT). Binding

efficiencies are expressed as the percent of cells positive for S1-Fc among the zsGreen positive cells (ACE2 expressing cells).

Production of SARS-CoV-2 or SARS-CoV pseudotyped virus

Pseudoviruses were produced in HEK293T cells by co-transfecting the retroviral vector pTG-MLV-Fluc, pTG-MLV-Gag-pol, and pcDNA3.1 expressing the SARS-CoV spike gene, SARS-CoV-2 spike gene or VSV-G (pMD2.G (Addgene #12259)) using VigoFect (Vigorous Biotechnology). At 48 h post transfection, the cell culture medium was collected for centrifugation at 3500 rpm for 10 min, and then the supernatant was subsequently aliquoted and stored at -80°C for further use. Virus entry was assessed by transduction of pseudoviruses in cells expressing ACE2 ortholog or mutants in 48-well plates. After 48 h, intracellular luciferase activity was determined using the Luciferase Assay System (Promega, Cat. #E1500) according to the manufacturer's instructions. Luminescence was recorded on a GloMax Discover System (Promega).

Analysis of SARS-CoV-2 infection by high-content imaging system

A549 cells were transduced with lentiviruses expressing the ACE2 of different species for 48 h. Cells were then infected with nCoV-SH01 (SARS-CoV-2) at an MOI of 1 for 1 h, washed three times with PBS, and incubated in 2% FBS culture medium for 48 h. Cell were then fixed for viral antigen staining with 4% paraformaldehyde in PBS, permeablized with 0.2% Triton X-100, and incubated with a rabbit polyclonal antibody against the SARS-CoV nucleocapsid protein (Rockland, 200-401-A50, 1μg/ml) and a mouse anti-FLAG M2 antibody (Sigma-Aldrich #1804, 1μg/ml) at 4°C overnight. After three washes, cells were incubated with a secondary goat anti-rabbit antibody conjugated with Alexa Fluor 555 (Thermo #A32732, 2 μg/ml) and goat anti-mouse antibody conjugated with Alexa Fluor 647 (Thermo #A21235, 2 μg/ml) for 2 h at room temperature, followed by staining with 4',6-diamidino-2-phenylindole (DAPI). Images were collected using an Operetta High-Content Imaging System (PerkinElmer). For high-content imaging, three biological replicates for each ACE2 ortholog/variant on different 96-well plates were scanned, and five representative fields were selected for each well. Image analysis was performed using the PerkinElmer Harmony high-content analysis software 4.9. ACE2-transduced cells were automatically identified by DAPI (nuclei) and zsGreen (cytoplasm, the lentiviral vector containing the ACE2 orthologs also expressed zsGreen). The mean fluorescent intensity (MFI) of the Alexa 647 (ACE2 orthologs) and Alexa 555 (viral nucleocapsid) channels were subsequently calculated for each cell. Cells with an Alexa 647 channel MFI >1000 were gated as ACE2-positive cells. ACE2-positive cells with an Alexa 555 channel MIF >1600 were gated as SARS-CoV-2-infected cells. The formula of SARS-CoV-2-infected cells/ ACE2-positive cells was followed as the readout for infection efficiency.

Generation and production of recombinant adenovirus expressing ACE2 variants

cDNA of human or mouse ACE2 variants with a FLAG tag at the C-terminus was cloned into pShuttle. The pShuttle-ACE2 plasmids were then electroporated into BJ5183 AD-1 cells (Agilent), which were pretransformed with pAdEasy-1 to facilitate recombination with the pShuttle-CMV vector. The adenovirus constructs were then transfected into HEK293 cells. The transfected HEK293 cells were maintained until the cells exhibited complete cytopathic effect (CPE) and then harvested and freeze-thawed. The supernatants were serially passaged two more times, with harvest at complete CPE and freeze-thaw. For virus purification, the cell pellets were purified using cesium chloride density-gradient ultracentrifugation, and the number

of virus particles was determined using a Nanodrop 2000 (Thermo Fisher Scientific). The adenovirus stocks were aliquoted and stored at -80°C.

SARS-CoV-2 infection of adenovirus transduced mice

Six to eight week-old male mice (BALB/c) were transduced intranasally with adenovirus expressing ACE2 variants respectively (5×10^{10} viral particles per mouse). After 3 days, mice were infected intranasally with SARS-CoV-2 (6×10^4 FFU per mouse) and sacrificed at day 3 post infection. The lung tissues were harvested for histopathological analysis and virus titration.

Histological analysis

Lung tissues were harvested and fixed in 4% paraformaldehyde (PFA) for 48 h. Tissues were embedded in paraffin for sectioning and stained with hematoxylin and eosin (H&E) to assess tissue morphology. To detect the expression of FLAG-tagged ACE2 delivered by adenovirus, the sections were incubated in blocking reagent and then with FLAG M2 antibody (1:100 dilution, Sigma-Aldrich #1804) at 4°C overnight, followed by incubation with HRP-conjugated goat anti-mouse IgG secondary antibody (1:5000 dilution, Invitrogen). The lung sections from the vector transduced mouse were used as negative control. For viral antigen detection, the sections were incubated with house-made mouse anti-SARS-CoV-2 nucleocapsid protein serum (1:5000) and HRP-conjugated goat anti-mouse IgG secondary antibody (1:5000 dilution, Invitrogen). The sections were observed under microscope (Olympus, Tokyo, Japan).

Virus load determination by focus-forming assay

Vero E6 monolayer in 96-well plates were inoculated with serially diluted virus for 2 h and then overlaid with methylcellulose for 48 h. Cells were fixed with 4% paraformaldehyde in PBS for 1 h and permeablized with 0.2% Triton X-100 for 1 h. Cells were stained with homemade mouse anti-SARS-CoV-2 N serum overnight at 4°C, incubated with the secondary goat anti-mouse HRP-conjugated antibody for 2 h at room temperature. The focus-forming unit was developed using TrueBlue substrate (Sera Care #5510–0030).

Statistical analysis

One-way analysis of variance (ANOVA) with Tukey's honestly significant difference (HSD) test was used to test for statistical significance of differences between the different group parameters. *P* values of less than 0.05 were considered statistically significant.

Supporting information

S1 Fig. Alignment of the counterpart residues of ACE2 orthologs at the interface of human ACE2 with the SARS-CoV-2 spike protein. Multiple ACE2 orthologs were retrieved from NCBI database and the counterpart residues of ACE2 orthologs at interfaces of human ACE2 with SARS-CoV-2 spike were aligned using MEGA. ACE2 orthologs highlighted in green were susceptible to SARS-CoV-2, and species highlighted in red were resistant to SARS-CoV-2. The restrictive residues of koala or mouse ACE2 are highlighted in red. (TIF)

S2 Fig. Gating strategy for determination of the binding efficiency of ACE2 variants with SARS-CoV-2 or SARS-CoV S1-Fc protein. (A-B) Main cell population was identified and gated on Forward and Side Scatter. Single cells were further gated on FSC-A and FSC-H. The gated cells were plotted by FITC-A (zsGreen, as the ACE2 expressing population) and APC-A

(S1-Fc bound population). The FITC-A positive cell population was plotted as a histogram to show the S1-Fc positive population as Fig 2B. The binding efficiency was defined as the percent of S1-Fc binding cells among the zsGreen positive cells. Shown are FACS plots representative of those that have been used for the calculations of binding efficiencies of ACE2 variants with S1-Fc. This experiment was independently repeated three times with similar results.
(ZIP)

S3 Fig. Expression and cell surface localization of ACE2 variants. (A) Western blotting assay was performed to detect expression of endogenous ACE2 in Calu-3 cells and ACE2 variants in A549 cells transduced by lentiviruses. (B) A549 cells transduced with lentiviruses (pLVX-IRES-zsGreen) expressing ACE2 variants were incubated with rabbit polyclonal antibody (Sino Biological Inc. China, Cat: 10108-T24) against ACE2. The cells were washed and then stained with 2μg/mL goat anti-rabbit IgG (H+L) conjugated with Alexa Fluor 568 for flow cytometry analysis. The cell surface ACE2 was calculated as the percent of Alex Fluor 568 positive cells among the zsGreen positive cells. This experiment was repeated three with similar result. (C) A549 cells transduced with lentiviruses (pLVX-IRES-zsGreen) expressing ACE2 variants were incubated with rabbit polyclonal antibody (Sino Biological Inc. China, Cat: 10108-T24) against ACE2. The cells were washed and then stained with 2μg/mL goat anti-rabbit IgG (H+L) conjugated with Alexa Fluor 568 and DAPI (1μg/ml). The cell images were captured with a Zeiss LSM 880 Confocal Microscope. ACE2 on cell surface was shown in the merge images processed by ZEN3.2 software. This experiment was independently repeated three with similar result and the representative images were shown. (D) Human, koala ACE2 or its variants cDNA was cloned as a carboxyl terminus fusion with EGFP. (E) A549 cells were transduced with lentivirus expressing ACE2 variant-EGFP proteins in (D) and cells were collected, washed and counterstained with DAPI (1μg/ml). The cell images were captured with a Zeiss LSM 880 Confocal Microscope. ACE2 on cell surface was shown in the merge images processed by ZEN3.2 software. This experiment was independently repeated three times with similar result and the representative images were shown.
(TIF)

S4 Fig. Human ACE2 mutants bind viral spike protein. (A) A549 cells were transduced with ACE2 orthologs or human ACE2 mutants as indicated, incubated with the recombinant S1 domain of the SARS-CoV-2 or SARS-CoV spike protein C-terminally fused with Fc, and then stained with goat anti-human IgG (H + L) conjugated to Alexa Fluor 647 for flow cytometry analysis. (B) The A549 cells transduced with ACE2 orthologs and their variants as indicated, and the cells were incubated with full-length spike protein of SARS-CoV-2 (SinoBiological, 40589-V08B1) or SARS-CoV (SinoBiological, 40634-V08B) C-terminally fused with His tag, and then stained with Anti-HIS-PE (Miltenyi Biotec#130-120-787). Values in (A) and (B) are expressed as the percent of cells positive for S1-Fc among the ACE2-expressing cells (zsGreen1 + cells) and shown as the means ± SD from 3 biological replicates. This experiments were independently performed three times with similar results.
(TIF)

Acknowledgments

Author Contributions

Conceptualization: Rong Zhang, Qiang Ding.

Data curation: Wenlin Ren, Xiaomin Zhao.

Formal analysis: Wenlin Ren, Rong Zhang, Qiang Ding.

Funding acquisition: Youhua Xie, Rong Zhang, Qiang Ding.

Investigation: Wenlin Ren, Yunkai Zhu, Yuyan Wang, Hongyang Shi, Yin Yu, Gaowei Hu, Fei Feng, Xiaomin Zhao, Jun Lan, Jianping Wu.

Methodology: Devin J. Kenney, Florian Douam, Rong Zhang, Qiang Ding.

Project administration: Rong Zhang, Qiang Ding.

Resources: Youhua Xie, Xinquan Wang, Zhenghong Yuan.

Software: Jianping Wu, Rong Zhang.

Supervision: Yimin Tong, Jin Zhong, Dongming Zhou, Rong Zhang, Qiang Ding.

Validation: Wenlin Ren, Yunkai Zhu, Rong Zhang, Qiang Ding.

Visualization: Wenlin Ren.

Writing – original draft: Wenlin Ren, Rong Zhang, Qiang Ding.

Writing – review & editing: Wenlin Ren, Jin Zhong, Rong Zhang, Qiang Ding.

References

1. Ksiazek TG, Erdman D, Goldsmith CS, Zaki SR, Peret T, Emery S, et al. A novel coronavirus associated with severe acute respiratory syndrome. N Engl J Med. 2003; 348(20):1953–66. Epub 2003/04/12. https://doi.org/10.1056/NEJMoa030781 PMID: 12690092.

2. Enjuanes L, Almazan F, Sola I, Zuniga S. Biochemical aspects of coronavirus replication and virus-host interaction. Annu Rev Microbiol. 2006; 60:211–30. Epub 2006/05/23. https://doi.org/10.1146/annurev.micro.60.080805.142157 PMID: 16712436.

3. Perlman S, Netland J. Coronaviruses post-SARS: update on replication and pathogenesis. Nat Rev Microbiol. 2009; 7(6):439–50. Epub 2009/05/12. https://doi.org/10.1038/nrmicro2147 PMID: 19430490; PubMed Central PMCID: PMC2830095.

4. Fehr AR, Perlman S. Coronaviruses: an overview of their replication and pathogenesis. Methods Mol Biol. 2015; 1282:1–23. Epub 2015/02/28. https://doi.org/10.1007/978-1-4939-2438-7_1 PubMed Central PMCID: PMC4369385. PMID: 25720466

5. Wu F, Zhao S, Yu B, Chen Y-M, Wang W, Song Z-G, et al. A new coronavirus associated with human respiratory disease in China. Nature. 2020; 579(7798):265–9. Epub 2020/02/06. https://doi.org/10.1038/s41586-020-2008-3 PMID: 32015508; PubMed Central PMCID: PMC7094943.

6. Zhou P, Yang XL, Wang XG, Hu B, Zhang L, Zhang W, et al. A pneumonia outbreak associated with a new coronavirus of probable bat origin. Nature. 2020; 579(7798):270–3. Epub 2020/02/06. https://doi.org/10.1038/s41586-020-2012-7 PMID: 32015507; PubMed Central PMCID: PMC7095418.

7. Cui J, Li F, Shi ZL. Origin and evolution of pathogenic coronaviruses. Nat Rev Microbiol. 2019; 17 (3):181–92. Epub 2018/12/12. https://doi.org/10.1038/s41579-018-0118-9 PMID: 30531947; PubMed Central PMCID: PMC7097006.

8. Zaki AM, van Boheemen S, Bestebroer TM, Osterhaus AD, Fouchier RA. Isolation of a novel coronavirus from a man with pneumonia in Saudi Arabia. N Engl J Med. 2012; 367(19):1814–20. Epub 2012/10/19. https://doi.org/10.1056/NEJMoa1211721 PMID: 23075143.

9. Morens DM, Fauci AS. Emerging Pandemic Diseases: How We Got to COVID-19. Cell. 2020; 182 (5):1077–92. Epub 2020/08/28. https://doi.org/10.1016/j.cell.2020.08.021 PubMed Central PMCID: PMC7428724. PMID: 32846157

10. Diamond MS, Pierson TC. The Challenges of Vaccine Development against a New Virus during a Pandemic. Cell Host Microbe. 2020; 27(5):699–703. Epub 2020/05/15. https://doi.org/10.1016/j.chom.2020.04.021 PMID: 32407708; PubMed Central PMCID: PMC7219397 and NGM Biopharmaceuticals,

and is on the Scientific Advisory Board of Moderna. The Diamond laboratory at Washington University School of Medicine has received sponsored research agreements from Moderna.

11. Douam F, Gaska JM, Winer BY, Ding Q, von Schaewen M, Ploss A. Genetic Dissection of the Host Tropism of Human-Tropic Pathogens. Annu Rev Genet. 2015; 49:21–45. Epub 2015/09/26. https://doi.org/10.1146/annurev-genet-112414-054823 PMID: 26407032; PubMed Central PMCID: PMC5075990.

12. Li F. Receptor recognition mechanisms of coronaviruses: a decade of structural studies. J Virol. 2015; 89(4):1954–64. Epub 2014/11/28. https://doi.org/10.1128/JVI.02615-14 PMID: 25428871; PubMed Central PMCID: PMC4338876.

13. Graham RL, Baric RS. Recombination, reservoirs, and the modular spike: mechanisms of coronavirus cross-species transmission. J Virol. 2010; 84(7):3134–46. Epub 2009/11/13. https://doi.org/10.1128/JVI.01394-09 PMID: 19906932; PubMed Central PMCID: PMC2838128.

14. Hoffmann M, Kleine-Weber H, Schroeder S, Kruger N, Herrler T, Erichsen S, et al. SARS-CoV-2 Cell Entry Depends on ACE2 and TMPRSS2 and Is Blocked by a Clinically Proven Protease Inhibitor. Cell. 2020; 181(2):271–80 e8. Epub 2020/03/07. https://doi.org/10.1016/j.cell.2020.02.052 PMID: 32142651; PubMed Central PMCID: PMC7102627.

15. Lu G, Wang Q, Gao GF. Bat-to-human: spike features determining 'host jump' of coronaviruses SARS-CoV, MERS-CoV, and beyond. Trends Microbiol. 2015; 23(8):468–78. Epub 2015/07/25. https://doi.org/10.1016/j.tim.2015.06.003 PMID: 26206723; PubMed Central PMCID: PMC7125587.

16. Bao L, Deng W, Huang B, Gao H, Liu J, Ren L, et al. The pathogenicity of SARS-CoV-2 in hACE2 transgenic mice. Nature. 2020; 583(7818):830–3. Epub 2020/05/08. https://doi.org/10.1038/s41586-020-2312-y PMID: 32380511.

17. Jiang RD, Liu MQ, Chen Y, Shan C, Zhou YW, Shen XR, et al. Pathogenesis of SARS-CoV-2 in Transgenic Mice Expressing Human Angiotensin-Converting Enzyme 2. Cell. 2020; 182(1):50–8 e8. Epub 2020/06/10. https://doi.org/10.1016/j.cell.2020.05.027 PMID: 32516571; PubMed Central PMCID: PMC7241398.

18. Sun S-H, Chen Q, Gu H-J, Yang G, Wang Y-X, Huang X-Y, et al. A Mouse Model of SARS-CoV-2 Infection and Pathogenesis. Cell Host & Microbe. 2020; 28(1):124–33.e4. Epub 2020/06/03. https://doi.org/10.1016/j.chom.2020.05.020 PMID: 32485164; PubMed Central PMCID: PMC7250783.

19. Sun J, Zhuang Z, Zheng J, Li K, Wong RL, Liu D, et al. Generation of a Broadly Useful Model for COVID-19 Pathogenesis, Vaccination, and Treatment. Cell. 2020; 182(3):734–43 e5. Epub 2020/07/10. https://doi.org/10.1016/j.cell.2020.06.010 PMID: 32643603; PubMed Central PMCID: PMC7284240.

20. Liu Y, Hu G, Wang Y, Zhao X, Ji F, Ren W, et al. Functional and Genetic Analysis of Viral Receptor ACE2 Orthologs Reveals a Broad Potential Host Range of SARS-CoV-2. bioRxiv. 2020:2020.04.22.046565. https://doi.org/10.1101/2020.04.22.046565

21. Li Y, Wang H, Tang X, Fang S, Ma D, Du C, et al. SARS-CoV-2 and three related coronaviruses utilize multiple ACE2 orthologs and are potently blocked by an improved ACE2-Ig. J Virol. 2020. Epub 2020/08/28. https://doi.org/10.1128/JVI.01283-20 PMID: 32847856.

22. Damas J, Hughes GM, Keough KC, Painter CA, Persky NS, Corbo M, et al. Broad host range of SARS-CoV-2 predicted by comparative and structural analysis of ACE2 in vertebrates. Proc Natl Acad Sci U S A. 2020; 117(36):22311–22. Epub 2020/08/23. https://doi.org/10.1073/pnas.2010146117 PMID: 32826334.

23. Lu S, Zhao Y, Yu W, Yang Y, Gao J, Wang J, et al. Comparison of nonhuman primates identified the suitable model for COVID-19. Signal Transduct Target Ther. 2020; 5(1):157. Epub 2020/08/21. https://doi.org/10.1038/s41392-020-00269-6 PMID: 32814760; PubMed Central PMCID: PMC7434851.

24. Lan J, Ge J, Yu J, Shan S, Zhou H, Fan S, et al. Structure of the SARS-CoV-2 spike receptor-binding domain bound to the ACE2 receptor. Nature. 2020; 581(7807):215–20. Epub 2020/04/01. https://doi.org/10.1038/s41586-020-2180-5 PMID: 32225176.

25. Wang Q, Zhang Y, Wu L, Niu S, Song C, Zhang Z, et al. Structural and Functional Basis of SARS-CoV-2 Entry by Using Human ACE2. Cell. 2020; 181(4):894–904.e9. Epub 2020/04/11. https://doi.org/10.1016/j.cell.2020.03.045 PMID: 32275855; PubMed Central PMCID: PMC7144619.

26. Shang J, Ye G, Shi K, Wan Y, Luo C, Aihara H, et al. Structural basis of receptor recognition by SARS-CoV-2. Nature. 2020; 581(7807):221–4. Epub 2020/04/01. https://doi.org/10.1038/s41586-020-2179-y PMID: 32225175; PubMed Central PMCID: PMC7328981.

27. Yan R, Zhang Y, Li Y, Xia L, Guo Y, Zhou Q. Structural basis for the recognition of SARS-CoV-2 by full-length human ACE2. Science. 2020; 367(6485):1444–8. Epub 2020/03/07. https://doi.org/10.1126/science.abb2762 PMID: 32132184.

28. Wan Y, Shang J, Graham R, Baric RS, Li F. Receptor Recognition by the Novel Coronavirus from Wuhan: an Analysis Based on Decade-Long Structural Studies of SARS Coronavirus. J Virol. 2020; 94

(7). Epub 2020/01/31. https://doi.org/10.1128/JVI.00127-20 PMID: 31996437; PubMed Central PMCID: PMC7081895.

29. Li W, Zhang C, Sui J, Kuhn JH, Moore MJ, Luo S, et al. Receptor and viral determinants of SARS-coronavirus adaptation to human ACE2. EMBO J. 2005; 24(8):1634–43. Epub 2005/03/26. https://doi.org/10.1038/sj.emboj.7600640 PMID: 15791205; PubMed Central PMCID: PMC1142572.

30. Li W, Wong SK, Li F, Kuhn JH, Huang IC, Choe H, et al. Animal origins of the severe acute respiratory syndrome coronavirus: insight from ACE2-S-protein interactions. J Virol. 2006; 80(9):4211–9. Epub 2006/04/14. https://doi.org/10.1128/JVI.80.9.4211-4219.2006 PMID: 16611880; PubMed Central PMCID: PMC1472041.

31. Li F, Li W, Farzan M, Harrison SC. Structure of SARS coronavirus spike receptor-binding domain complexed with receptor. Science. 2005; 309(5742):1864–8. Epub 2005/09/17. https://doi.org/10.1126/science.1116480 PMID: 16166518.

32. Blanco-Melo D, Nilsson-Payant BE, Liu WC, Uhl S, Hoagland D, Moller R, et al. Imbalanced Host Response to SARS-CoV-2 Drives Development of COVID-19. Cell. 2020; 181(5):1036–45 e9. Epub 2020/05/18. https://doi.org/10.1016/j.cell.2020.04.026 PMID: 32416070; PubMed Central PMCID: PMC7227586.

33. Sun J, Zhuang Z, Zheng J, Li K, Wong RL-Y, Liu D, et al. Generation of a Broadly Useful Model for COVID-19 Pathogenesis, Vaccination, and Treatment. Cell. 2020; 182(3):734-43.e5. Epub 2020/07/10. https://doi.org/10.1016/j.cell.2020.06.010 PMID: 32643603; PubMed Central PMCID: PMC7284240.

34. Hassan AO, Case JB, Winkler ES, Thackray LB, Kafai NM, Bailey AL, et al. A SARS-CoV-2 Infection Model in Mice Demonstrates Protection by Neutralizing Antibodies. Cell. 2020; 182(3):744–53 e4. Epub 2020/06/20. https://doi.org/10.1016/j.cell.2020.06.011 PMID: 32553273; PubMed Central PMCID: PMC7284254.

35. Li F. Structural analysis of major species barriers between humans and palm civets for severe acute respiratory syndrome coronavirus infections. J Virol. 2008; 82(14):6984–91. Epub 2008/05/02. https://doi.org/10.1128/JVI.00442-08 PMID: 18448527; PubMed Central PMCID: PMC2446986.

36. Structure Li F., Function, and Evolution of Coronavirus Spike Proteins. Annu Rev Virol. 2016; 3(1):237–61. Epub 2016/09/01. https://doi.org/10.1146/annurev-virology-110615-042301 PMID: 27578435; PubMed Central PMCID: PMC5457962.

37. Zhao X, Chen D, Szabla R, Zheng M, Li G, Du P, et al. Broad and Differential Animal Angiotensin-Converting Enzyme 2 Receptor Usage by SARS-CoV-2. J Virol. 2020; 94(18). Epub 2020/07/15. https://doi.org/10.1128/JVI.00940-20 PMID: 32661139; PubMed Central PMCID: PMC7459545.

38. Gu H, Chen Q, Yang G, He L, Fan H, Deng YQ, et al. Adaptation of SARS-CoV-2 in BALB/c mice for testing vaccine efficacy. Science. 2020; 369(6511):1603–7. Epub 2020/08/01. https://doi.org/10.1126/science.abc4730 PMID: 32732280; PubMed Central PMCID: PMC7574913.

39. Oude Munnink BB, Sikkema RS, Nieuwenhuijse DF, Molenaar RJ, Munger E, Molenkamp R, et al. Transmission of SARS-CoV-2 on mink farms between humans and mink and back to humans. Science. 2021; 371(6525):172–7. Epub 2020/11/12. https://doi.org/10.1126/science.abe5901 PMID: 33172935.

40. Saitou N, Nei M. The neighbor-joining method: a new method for reconstructing phylogenetic trees. Mol Biol Evol. 1987; 4(4):406–25. Epub 1987/07/01. https://doi.org/10.1093/oxfordjournals.molbev.a040454 PMID: 3447015.